
ENHANCING CROSS-VIEW UAV GEOLOCALIZATION VIA LVLM-DRIVEN RELATIONAL MODELING

Bowen Liu*

Department of Data Science
City University of Hong Kong
Hong Kong

boweliu6-c@my.cityu.edu.hk

Pengyue Jia*

Department of Data Science
City University of Hong Kong
Hong Kong

jia.pengyue@my.cityu.edu.hk

Wanyu Wang

Information System
City University of Hong Kong
Hong Kong

wanyuwang4-c@my.cityu.edu.hk

Derong Xu

Department of Data Science
City University of Hong Kong
Hong Kong

derongxu2-c@my.cityu.edu.hk

Jiawei Cheng

Department of Data Science
City University of Hong Kong
Hong Kong

jiawcheng5-c@my.cityu.edu.hk

Jiancheng Dong

Department of Data Science
City University of Hong Kong
Hong Kong

jiancdong2-c@my.cityu.edu.hk

Xiao Han

College of Computer Science and Technology
Zhejiang University of Technology
Zhejiang

hahahenha@gmail.com

Zimo Zhao

Department of Data Science
City University of Hong Kong
Hong Kong

zmzhao6-c@my.cityu.edu.hk

Chao Zhang

Department of Data Science
City University of Hong Kong
Hong Kong

czhang2328-c@my.cityu.edu.hk

Bowen Yu

Department of Data Science
City University of Hong Kong
Hong Kong

bowyu2-c@my.cityu.edu.hk

Fangyu Hong

Department of Data Science
City University of Hong Kong
Hong Kong

fangyuhong2-c@my.cityu.edu.hk

Xiangyu Zhao[†]

Department of Data Science
City University of Hong Kong
Hong Kong

xianzhao@cityu.edu.hk

ABSTRACT

The primary objective of cross-view UAV geolocation is to identify the exact spatial coordinates of drone-captured imagery by aligning it with extensive, geo-referenced satellite databases. Current approaches typically extract features independently from each perspective and rely on basic heuristics to compute similarity, thereby failing to explicitly capture the essential interactions between different views. To address this limitation, we introduce a novel, plug-and-play ranking architecture designed to explicitly perform joint relational modeling for improved UAV-to-satellite image matching. By harnessing the capabilities of a Large Vision-Language Model (LVLM), our framework effectively learns the deep visual-semantic correlations linking UAV and satellite imagery. Furthermore, we present a novel relational-aware loss function to optimize the training phase. By employing soft labels, this loss provides fine-grained supervision that avoids overly penalizing near-positive matches,

*Equal contribution

[†]Corresponding author

ultimately boosting both the model’s discriminative power and training stability. Comprehensive evaluations across various baseline architectures and standard benchmarks reveal that the proposed method substantially boosts the retrieval accuracy of existing models, yielding superior performance even under highly demanding conditions.

Keywords Cross-view geolocalization · LVLM · UAV

1 Introduction

Cross-view geolocalization for unmanned aerial vehicles (UAVs) involves estimating the geographic position of a UAV-captured image by matching it to a reference database of geo-tagged overhead imagery, such as satellite views [1]. This task has emerged as a critical alternative to satellite-based navigation systems (e.g., GPS [2]), which may fail in contested environments due to signal jamming or environmental interference. By exploiting visual cues from disparate viewpoints, cross-view geolocalization offers a robust solution in scenarios where conventional methods are unreliable, enabling applications in autonomous navigation [3, 4], disaster response [5, 6], precision agriculture [7], and urban planning [8]. However, the task remains challenging due to the significant domain gap between UAV-oblique and satellite-orthographic images, including differences in scale, illumination, occlusion, and seasonal appearance [9]. Addressing these discrepancies requires advanced feature matching and domain adaptation techniques.

Recent progress [10, 11, 12] in cross-view UAV geolocalization has primarily relied on dual-stream architectures, where separate encoders process UAV-oblique and satellite-orthographic images to extract view-specific features. During inference, these methods retrieve a set of candidates from the satellite image pool and select the one with the highest similarity score as the final location prediction. While existing methods explore various backbone networks—including convolutional neural networks [13, 14, 9], Transformers [15, 12], and state space models [16]—to improve representation learning, they all eventually fall back to naive heuristics (e.g., cosine similarity [17]) for scoring cross-view relevance. This heuristic ranking strategy ignores the intricate semantic and spatial relationships between UAV and satellite views, which are essential for closing the large domain gap and improving candidate selection accuracy. Moreover, current contrastive learning based training objectives, including InfoNCE [18] and triplet loss [19], impose uniform penalties on all negative pairs, regardless of their visual or geographic proximity to the ground truth. This overly rigid supervision can hinder convergence and reduce discriminative ability in challenging scenarios, ultimately constraining model robustness and generalization.

To address the aforementioned limitations, we introduce SkyLink, a novel ranking framework that explicitly joins relational modeling for cross-view UAV geolocalization. Unlike previous methods that model UAV and satellite views separately, SkyLink leverages an LVLM to jointly model the cross-view interaction in a unified representation space and directly outputs a scalar relevance score for each candidate.

This unified modeling enables the network to capture semantic correspondences and spatial alignments across views, which are often missed by independent encoders followed by naive similarity measures. Furthermore, we propose a novel relational-aware loss that incorporates soft labels to provide nuanced supervision, assigning graduated penalties to near-positive pairs. This design stabilizes the training process and ultimately leads to improved performance.

Addressing the lack of datasets dedicated to training ranking models, we curated SkyRank from open-source benchmarks. We first employ an existing cross-view geolocalization model as a retriever to generate candidate sets from a large satellite image pool for each UAV query image. The ground truth is either present in the retrieved candidates or explicitly inserted, ensuring that the model learns to identify the correct match from among them. While this preprocessing introduces a specific inductive bias, this intentional distribution shift aligns the training distribution with that of the inference phase. This alignment compels the model to focus on distinguishing hard samples that share global similarities yet differ. To support future research in cross-view geolocalization and broader vision-language tasks, we will release SkyRank.

This paper validates the effectiveness of the proposed method by evaluating SkyLink under task settings, based on combinations of three retrievers (Sample4geo [13], SDPL [20], MCGG [21]) and two benchmark datasets (University-1652 [22], SUES-200 [23]). The results demonstrate that the retriever combinations with SkyLink as a plugin achieve comprehensive improvements in metrics such as recall rate and average precision. Furthermore, extensive ablation studies confirm the effectiveness of each proposed component, while hyperparameter sensitivity analysis provides profound insights into model stability. Our contributions can be summarized as follows:

- We propose SkyLink, a novel plug-and-play LVLM-based framework for cross-view UAV geolocalization that jointly models interactions across UAV and satellite views within a unified representation space. This joint

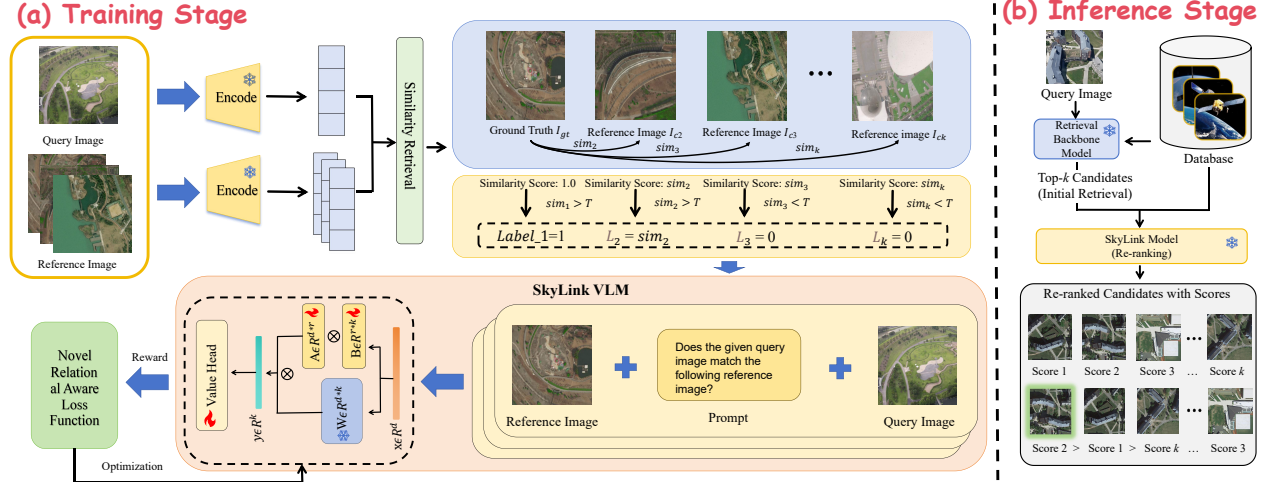


Figure 1: The Framework of SkyLink. During the training phase, the model takes the retrieval results generated by the retriever on the training set as input. In the inference phase, the model receives the retrieval results output by the retriever on the test set, and optimizes them through re-ranking.

modeling improves relevance scoring via fine-grained cross-view correspondences, overcoming limitations of prior heuristic measures in the literature.

- We construct and release SkyRank datasets for cross-view geolocation. SkyRank is curated to support the training of ranking-based methods. By releasing this derived benchmark, we aim to provide a useful resource for further exploration in cross-view geolocation and related fields.
- Extensive experiments are conducted within a single task setting, involving combinations of three retrievers and two benchmark datasets. The results demonstrate that SkyLink comprehensively enhances the retrieval performance of the retrievers.
- We propose a novel dynamic relation-aware loss function, which leverages soft labels to deliver more granular supervisory signals and mitigates the severe penalty imposed on near-positive pairs.

2 Methodology

In this section, we introduce SkyLink, our proposed ranking framework for cross-view UAV geolocation that explicitly models the interaction between different views. As illustrated in Figure 1, the overall framework of SkyLink comprises two main stages: training stage and inference stage.

2.1 Dataset Curation

Since no off-the-shelf dataset is available for training ranking models in cross-view geolocation, we construct new datasets from existing public benchmarks to support the training of SkyLink. Given a standard cross-view geolocation dataset, we denote a query UAV image as I_q , its corresponding ground truth satellite image as I_{gt} , and the entire pool of reference satellite images as $\mathcal{R} = \{I_{r_i}\}_{i=1}^N$.

To generate a set of candidate images for each query, we first employ a pre-trained cross-view geolocation model as a retriever. We build a feature gallery $\mathcal{V}_{\mathcal{R}}$ by encoding every reference image $I_{r_i} \in \mathcal{R}$ using the retriever’s reference encoder $\mathcal{E}_r(\cdot)$, such that $\mathcal{V}_{\mathcal{R}} = \{\mathbf{v}_{r_i} | \mathbf{v}_{r_i} = \mathcal{E}_r(I_{r_i})\}$. For each query image I_q , we extract its feature vector $\mathbf{v}_q = \mathcal{E}_q(I_q)$. We then retrieve the top- m most similar candidates \mathcal{C}_q from the reference pool by matching all reference features based on their cosine similarity to the query feature:

$$\mathcal{C}_q = \left\{ I_{r_i} \mid I_{r_i} \in \underset{I_{r_j} \in \mathcal{R}}{\text{top-}m \text{ sim}}(\mathbf{v}_q, \mathbf{v}_{r_j}) \right\}, \quad (1)$$

where we define the similarity function as the cosine similarity $\text{sim}(\mathbf{v}_q, \mathbf{v}_{r_i}) = \mathbf{v}_q^\top \mathbf{v}_{r_i} / \|\mathbf{v}_q\| \|\mathbf{v}_{r_i}\|$.

The retrieved set C_q contains hard negative samples but may or may not include the ground truth I_{gt} . To handle these scenarios, we curate the candidate set C'_q as follows:

$$C'_q = \begin{cases} C_q \setminus \{I_{gt}\}, & \text{if } I_{gt} \in C_q \\ C_q \setminus \{I_{r_m}\}, & \text{if } I_{gt} \notin C_q \end{cases}, \quad (2)$$

where I_{r_m} is the least similar (the m -th) candidate in C_q . This process ensures that C'_q consistently contains exactly $m - 1$ candidates for every query. Finally, each sample in our curated dataset consists of a tuple containing the query image I_q , the set of $m - 1$ candidates C'_q , and the ground truth image I_{gt} .

2.2 SkyLink

Existing approaches [13, 14, 9] typically adopt a dual-stream architecture, where images from different views are encoded separately and then projected into a shared representation space. The final candidates are selected based on the similarity between these representations. While substantial effort has been devoted to improving feature extraction within each stream, much less attention has been paid to modeling the interactions across different views. The commonly used naive heuristics (e.g., cosine similarity) often fail to capture the complex semantic and spatial relationships between views, resulting in suboptimal matching performance. To address this limitation, we propose SkyLink, a novel ranking framework that explicitly models cross-view interactions. Specifically, images from different views are first combined using a predefined prompt template to form a unified model input. SkyLink then leverages a powerful LVLM backbone to capture the intricate relationships across views. Finally, a value head is appended to the last layer of the LVLM to produce a scalar relevance score, which reflects the matching degree between the query and candidate images.

Cross-View Prompt Template. To leverage LVLMs, we integrate multi-view images into a unified input. Given a sample (I_q, C'_q, I_{gt}) , we employ a hard negative mining strategy rather than random sampling. Specifically, we select the top- $(k - 1)$ candidates from C'_q based on retriever similarity. These 'hard negatives'—visually similar to I_q yet geographically distinct—are combined with I_{gt} to form the candidate set. This design compels the model to distinguish among highly ambiguous samples. For each candidate in this set, together with the query image I_q , we construct an input using the following prompt template: <query image> *Does the given query image match the following reference image?* <candidate image>

As a result, each training sample yields k prompt inputs. Formally, this process can be expressed as:

$$\mathcal{P} = \{ \text{Prompt}(I_q, I_{c_j}) \mid I_{c_j} \in \{I_{gt}\} \cup \text{top-}(k - 1)(C'_q) \}, \quad (3)$$

where $\text{Prompt}(\cdot, \cdot)$ denotes the application of the cross-view template to a query–candidate pair.

Model Architecture. The constructed prompt set \mathcal{P} is fed into a pretrained LVLM backbone to capture the semantic and spatial interactions between the query and candidate images. To adapt the model to the cross-view matching task, we insert Low-Rank Adaptation (LoRA) [24] modules into each transformer layer of the LVLM. These lightweight adapters enable efficient fine-tuning and improve the model’s expressiveness over multi-view inputs. Specifically, for a given transformer layer l , we apply LoRA to the projection matrix \mathbf{W}_l as follows:

$$\tilde{\mathbf{W}}_l = \mathbf{W}_l + \Delta \mathbf{W}_l = \mathbf{W}_l + \mathbf{A}_l \mathbf{B}_l, \quad (4)$$

where $\tilde{\mathbf{W}}_l \in \mathbb{R}^{d \times d}$ is the updated weight matrix, $\mathbf{W}_l \in \mathbb{R}^{d \times d}$ is the original frozen weight matrix from the LVLM, and $\mathbf{A}_l \in \mathbb{R}^{d \times r}$, $\mathbf{B}_l \in \mathbb{R}^{r \times d}$ are the trainable low-rank matrices with $\text{rank } r \ll d$. During training, only \mathbf{A}_l and \mathbf{B}_l are updated, enabling efficient adaptation to the cross-view matching task with minimal additional parameters.

We extract the hidden state of the last token from the final layer of the LVLM as a compact summary of the cross-view input. To produce a scalar relevance score, we apply a lightweight value head—implemented as a single bias-free linear layer—on top of this representation:

$$S = \mathbf{w}^\top \mathbf{h}_{[\text{last}]}, \text{ where } \mathbf{h}_{[\text{last}]} = \text{LVLM}(\mathcal{P})_{[-1]}, \quad (5)$$

where $S \in \mathbb{R}^k$ is the output score vector for the k candidates, \mathbf{w} is the weight vector of the value head, and $\mathbf{h}_{[\text{last}]}$ denotes the hidden state of the last token from the final layer of the LVLM. The resulting score reflects the predicted matching degree between the query and candidate image pair.

2.3 Relational-aware Optimization

Previous works [25, 13, 14, 9, 26], constrained by their dual-stream architectures, typically rely on InfoNCE or triplet loss to optimize separate encoders for each view. However, these objectives are not only ill-suited for training a ranking

framework like SkyLink, but also share a critical limitation: they penalize all negative samples uniformly, failing to account for their visual or geographic proximity to the ground truth. Such rigid supervision can impair model convergence and diminish its discriminative power in challenging scenarios. To address these limitations, we propose a novel relational-aware loss function to train SkyLink. This loss is designed to guide the model in selecting the correct match from a list of candidates while providing soft labels to near-positive examples, which significantly enhances training stability.

Training Objective. Given the output score vector $S \in \mathbb{R}^k$ from the LVLM and the candidate set $C'_q = \{I_{c_1}, I_{c_2}, \dots, I_{c_k}\}$, along with the ground-truth reference image I_{gt} and the retriever’s reference encoder \mathcal{E}_r , we construct soft labels based on the similarity between each candidate and the ground truth in the feature space. Specifically, for each candidate image $I_{c_j} \in C'_q$, we compute its cosine similarity with the ground-truth image:

$$\text{sim}_j = \frac{\mathcal{E}_r(I_{c_j})^\top \mathcal{E}_r(I_{gt})}{\|\mathcal{E}_r(I_{c_j})\| \cdot \|\mathcal{E}_r(I_{gt})\|}, \quad (6)$$

It is worth noting that, due to the way we construct the dataset, the candidate set C'_q is guaranteed to contain the ground truth image I_{gt} , whose similarity score is always 1.0. We then define a soft label vector $L \in \mathbb{R}^k$ as follows:

$$L_j = \begin{cases} \text{sim}_j, & \text{if } \text{sim}_j > T, \\ 0, & \text{otherwise,} \end{cases} \quad (7)$$

where T is a similarity threshold that filters out unrelated candidates.

We train the model using the binary cross-entropy loss with logits. The loss is computed between the predicted scores S and the soft labels L as follows:

$$\mathcal{L} = -\frac{1}{k} \sum_{j=1}^k [L_j \cdot \log \sigma(S_j) + (1 - L_j) \cdot \log(1 - \sigma(S_j))], \quad (8)$$

where $\sigma(\cdot)$ denotes the sigmoid function. This formulation allows the model to learn fine-grained cross-view relevance supervision based on feature-space proximity, rather than relying on binary labels alone.

2.4 Inference

Inference. During inference, we first retrieve a candidate set C_q from the reference image pool based on the query image I_q . Each query–candidate pair (I_q, I_{c_j}) is then used to construct an input prompt according to the predefined template. These prompts are fed into the SkyLink model to compute a matching score for each pair:

$$s_j = \text{SkyLink}(\text{Prompt}(I_q, I_{c_j})), \quad \text{for } I_{c_j} \in C_q. \quad (9)$$

Then, we select the candidate with the highest score as the predicted match:

$$\hat{I} = \arg \max_{I_{c_j} \in C_q} s_j. \quad (10)$$

This inference procedure enables accurate cross-view geolocalization by ranking the candidates based on their semantic and spatial relevance to the query.

3 Experiments

3.1 Experimental Setup

Datasets and Evaluation Metrics. We conduct experiments on two datasets of cross-view geolocalization tasks. The experiment is an image-based UAV geolocalization task, for which we use two widely adopted benchmark datasets: University-1652 [22] and SUES-200 [23]. Following the original dataset protocols, we evaluate performance using Recall and Average Precision (AP). For specific details regarding the datasets and evaluation metrics, please refer to Appendix A.1.

Table 1: Comprehensive Performance Comparison on University-1652 and SUES-200 Datasets Based on Various Retrievers.

Method	University-1652						SUES-200 Dataset							
	D2S			S2D			150m		200m		250m		300m	
	R@1	R@5	AP	R@1	R@5	AP	R@1	AP	R@1	AP	R@1	AP	R@1	AP
SDPL [20]	85.17	94.96	89.61	89.30	92.87	89.49	79.65	83.03	86.48	89.08	93.33	94.70	93.15	94.53
+SkyLink (Ours)	93.87	96.57	95.13	91.87	93.44	91.57	90.97	93.15	94.13	96.39	94.57	96.76	94.65	96.44
<i>Improvement</i> ¹	↑8.70	↑1.61	↑5.52	↑2.57	↑0.57	↑2.08	↑11.32	↑10.12	↑7.65	↑7.31	↑1.24	↑2.06	↑1.50	↑1.91
MCCG [21]	89.58	96.55	92.72	93.44	96.29	93.93	76.20	84.49	89.42	93.54	94.45	96.55	96.75	98.25
+SkyLink (Ours)	94.93	97.79	96.27	93.58	97.15	94.49	93.37	95.03	95.67	97.36	96.50	97.78	97.52	98.52
<i>Improvement</i> ¹	↑5.35	↑1.24	↑3.55	↑0.14	↑0.86	↑0.56	↑17.17	↑10.54	↑6.25	↑3.82	↑2.05	↑1.23	↑0.77	↑0.27
Sample4geo [13]	92.05	97.55	94.49	94.58	96.72	94.82	92.87	95.58	94.47	96.79	96.83	98.17	97.40	98.16
+SkyLink (Ours)	95.28	98.05	96.56	94.58	96.72	94.82	95.77	97.51	96.45	98.02	97.75	98.70	97.62	98.76
<i>Improvement</i> ¹	↑3.23	↑0.50	↑2.07	↑0.00	↑0.00	↑0.00	↑2.90	↑1.93	↑1.98	↑1.23	↑0.92	↑0.53	↑0.22	↑0.60

¹Improvement in model performance and baseline comparison.

SkyRank Dataset. In this study, we curated a derived dataset tailored for training candidate ranking models in cross-view geolocalization. Specifically, for each UAV query image, we retrieved a set of candidate samples based on the embedding similarity derived from the training set with a retriever (cross-view geolocalization model). Subsequently, we ensured the presence of the ground-truth match in each candidate set by either retaining it if already retrieved or explicitly inserting it during the subsequent data cleaning process. For each combination of retrievers, we constructed a corresponding re-ranking dataset. The purpose of releasing this dataset is to provide support for the development of cross-view geolocalization and related research fields, such as UAV navigation, information retrieval, and large vision-language models (LVLMs). For example entries of the dataset, please refer to Appendix A.2.

Implementation Details. Our retriever is built upon three state-of-the-art cross-view geo-localization retrievers: SDPL [20], Sample4Geo [13] and MCCG [21]. (For more details of retrievers, refer to Appendix A.3) During the training phase, 20 candidate samples are retrieved from the database for each query sample. Among these, the top-13 samples are used as retrieval candidate samples. In SkyLink, Qwen2-VL-7b-Instruct is adopted as the backbone network of the Large Vision-Language Model (LVLM). For LoRA (Low-Rank Adaptation) fine-tuning, the target modules include q_proj , k_proj , v_proj , and visual LoRA. SkyLink is fine-tuned using the AdamW [27] optimizer. All experiments are conducted based on the PyTorch framework and completed on 2 NVIDIA A100 GPUs (80GB). In the inference phase, the retrievers are used to generate candidate samples for the LVLM. The similarity threshold T is set to 0.9; Throughout the entire inference phase, re-ranking is only performed on the top-10 reference images retrieved by the retrievers. Additional details on the training environment and runtime are provided in Appendix A.4.

3.2 Main Results

To systematically evaluate the generality and incremental optimization potential of the SkyLink model as a plug-and-play re-ranking module, this study conducted comprehensive and rigorous comparative experiments on multiple representative geospatial image retrieval benchmark datasets with different base retrievers. As shown in Table 1, after re-ranking by the SkyLink model, all base retrievers achieved significant performance improvements on datasets such as University-1652 and SUES-200. For example, in the drone-to-street (D2S) task, the model exhibited particularly prominent enhancement effects on systems with SDPL and MCCG as base retrievers — it improved the R@1 metric of SDPL by 8.7% in the University-1652 dataset and further boosted the recall rate of MCCG by 17.17% in the 150m low-altitude drone retrieval task on the SUES-200 dataset, fully demonstrating its excellent performance optimization potential. Notably, although MCCG [21] and Sample4Geo [13] among the retrievers have shown relatively superior retrieval performance, the inherent modal information isolation of the traditional dual-stream architecture and the intrinsic limitation of the InfoNCE loss function in distinguishing ambiguous samples restrict their performance upper bound. In contrast, the SkyLink model breaks through the above bottlenecks through two core innovations: firstly, it abandons the modal isolation constraint of the traditional dual-stream architecture and constructs a cross-modal image-text interaction mechanism; secondly, it proposes a novel dynamic relation-aware loss function, which achieves accurate distinction of ambiguous samples via a soft-label modeling strategy, thereby significantly improving the retrieval accuracy in the re-ranking stage. In summary, our method yields substantial improvements in retrieval performance of retrievers across all datasets, fully verifying its effectiveness and superiority.

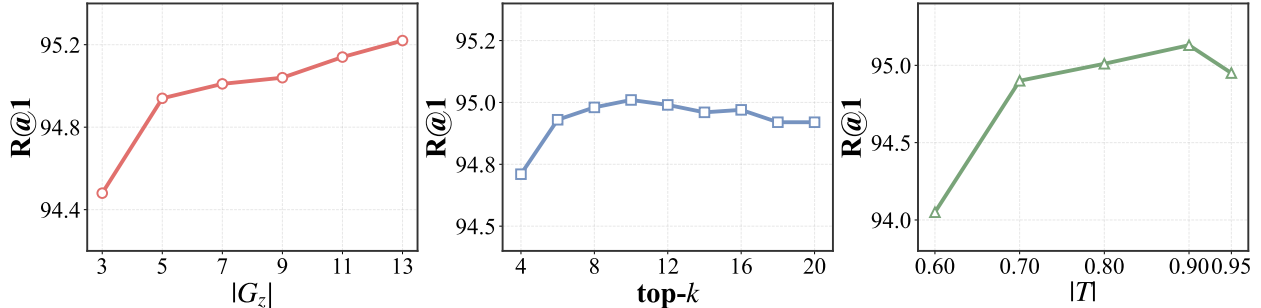


Figure 2: Hyperparameter Analysis on University-1652.

Table 2: Ablation Study and Parameter Scale Analysis on University-1652.

(a) Ablation Study.				(b) Parameter Scale Analysis.			
Method	R@1 \uparrow	R@5 \uparrow	AP \uparrow	Backbone model	R@1 \uparrow	R@5 \uparrow	AP \uparrow
Ours	95.28	98.05	96.56	llava-onevision-0.5B	90.61	97.94	93.92
w/o soft positive label	<u>95.13</u>	<u>98.03</u>	<u>96.47</u>	Qwen2-VL-2B-Instruct	91.18	97.96	94.25
w/o similarity threshold	94.07	98.08	95.94	Qwen2-VL-7B-Instruct	95.28	98.05	96.56
w/o SkyLink	92.05	97.55	94.49	Improvement ¹	\uparrow 4.67	\uparrow 0.11	\uparrow 2.64

¹Maximum performance gain among models.

3.3 Hyperparameter Analysis

To gain an in-depth understanding of the impact of key hyperparameters, we conducted systematic ablation experiments following the experimental method of controlling variables. The hyperparameters under consideration include: (1) The number of retrieval candidates G_z in the training phase; (2) The number of retrieval candidates (top- k) in the inference phase; (3) The similarity threshold T for soft classification. Unless otherwise specified, the default parameter values are set as follows: $|G_z| = 7$, top- $k = 10$, and $|T| = 0.8$ in this section. All experiments were implemented using Sample4geo as the retriever, with the University-1652 dataset serving as the experimental benchmark. Due to hardware constraints, the maximum value of $|G_z|$ was limited to 13.

We conduct a systematic analysis of the experimental results presented in Figure 2.

Regarding the candidate size $|G_z|$ in the training phase, the model performance exhibits a continuous upward trend as $|G_z|$ increases. This phenomenon can be attributed to the following: a moderate expansion of the candidate pool elevates the task complexity during the training process—by introducing more diverse reference samples, the model gains access to richer supervisory signals. These supervisory signals facilitate the model in learning fine-grained feature representations and discriminative decision boundaries, thereby enhancing its generalization ability on the target task. For the retrieval candidate size top- k in the inference phase, the model performance shows a ‘first rising and then stabilizing’ trajectory. In the initial stage of top- k increase, a larger candidate pool directly improves the probability of including the ground-truth candidate in the retrieval results, thus driving the continuous improvement of evaluation metrics. However, when top- k exceeds a specific threshold, the expanded candidate pool inevitably introduces a large number of noisy samples (i.e., irrelevant candidates with low feature similarity to the query sample). Notably, even in the presence of such noise, the model performance remains stable, which strongly demonstrates that the proposed model possesses robust anti-noise capability. This robustness stems from the model’s effective feature filtering mechanism: during the re-ranking process, the model can prioritize the identification of high-confidence relevant candidates while suppressing the interference of noisy samples, ultimately maintaining reliable inference performance.

For the similarity threshold ($|T|$), the model performance exhibits a significant ‘first increasing and then decreasing’ trend, with its optimal performance achieved when $|T| = 0.9$. This phenomenon reveals that applying an appropriate penalty constraint on sample labels can effectively guide the model to explore the latent distribution patterns and feature correlations of similar samples in the candidate pool, thereby enhancing the model’s ability to discriminate samples with subtle differences. This result demonstrates that by dynamically adjusting the constraint strength on sample similarity, a potential solution with both interpretability and practicality can be provided for the academic challenge of fine-grained distinction between positive samples and semi-positive samples. Notably, the selection of the hyperparameter $|T|$ exhibits flexibility and can be adaptively adjusted based on the structural distribution of specific datasets. For further details on hyperparameter $|T|$, please refer to Appendix A.5

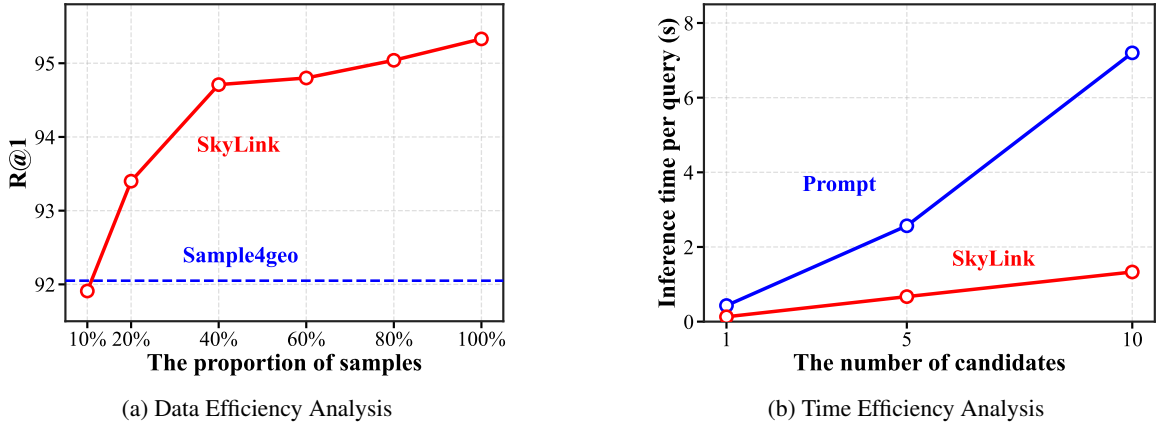


Figure 3: Efficiency analysis on University-1652.

3.4 Ablation Study

To deeply analyze the functional contributions and action mechanisms of each core component in the model, this study conducted ablation experiments using the systematic component removal method.

The specific experimental settings of ablation study are defined as follows:

- **w/o soft positive label:** Refers to the adoption of a hard label encoding mechanism in the model training process. When the cosine similarity between reference samples in the training set exceeds a preset similarity threshold, the label of the sample pair is directly hard-coded as 1, without introducing an elastic space for soft label classification.
- **w/o similarity threshold:** Refers to the exclusion of a penalty threshold mechanism based on cosine similarity during model training, i.e., no soft label classification based on similarity is performed for sample labels, and only a unified label definition method is adopted.
- **w/o SkyLink:** Refers to the complete removal of the SkyLink model, retaining only the baseline retrieval capability of the retriever.

Table 2(a) presents the ablation experiment results of the proposed model on the University-1652 dataset. Based on the data in the table, the following key conclusions can be drawn:

1. All core components in the model framework make significant positive contributions to the final performance of the model. This result directly verifies the rationality and effectiveness of the model design scheme proposed in this study.
2. A performance comparison between the complete model and the variant model with the soft encoding strategy removed shows that: within the reference sample range of the training set, the category discrimination ability of the variant model for ambiguous samples, positive samples, and semi-positive samples is significantly lower than that of the complete model. This phenomenon indicates that the flexible label encoding strategy can effectively enhance the model’s ability to identify and distinguish ambiguous samples during the training phase, while providing more flexible technical support for exploring the potential correlations within the reference set and between reference samples.
3. After removing the similarity threshold mechanism from the model, the experiment observed a phenomenon of severe fluctuations in the loss value during the entire training process of the model. Please refer to Appendix A.6 for details on the further analysis.

3.5 Efficiency Analysis

In addition to accuracy, parameter scale and efficiency are also indispensable key indicators in practical deployment scenarios. The study, based on the University-1652 dataset, evaluates the performance of the proposed SkyLink method across three dimensions: parameter scale, time efficiency (measured by inference latency), and data efficiency (assessed by the effectiveness of data utilization).

In the parameter scale analysis, Table 2(b) presents the comparative results of inference accuracy for the SkyLink method using llava-onevision-0.5B [28], Qwen2-VL-2B-Instruct [29] and Qwen2-VL-7B-Instruct [30] as backbone models, respectively. The experimental results align with expectations: as the parameter scale of the backbone model increases, the inference accuracy of larger-parameter models consistently outperforms that of smaller-parameter models, indicating that a higher parameter scale contributes to enhancing the model’s understanding of task semantics and its capability to capture image features.

In the time efficiency analysis, we adopt a prompt-based method (Appendix A.8 for details) as the baseline: the query image and all candidate images retrieved by Sample4geo are incorporated into the prompt, which is then used to guide the LVLm to select the most appropriate candidate as the final prediction. As Figure 3b shows, inference time increases with candidate count (1→10) for both methods (Skylink incurs computational overhead from additional scoring iterations, whereas the prompting-based baseline suffers from the need to construct progressively longer prompts.), yet Skylink maintains sub-second latency—under one-fifth that of the prompt-based approach. This stems from Skylink’s parallel evaluation architecture, which avoids the near-exponential latency growth of sequential prompt processing. Skylink natively supports large-scale parallel scoring, while the prompt-based method is inherently limited by its sequential input construction, making Skylink highly efficient for large-scale retrieval.

In the data efficiency analysis, Figure 3a illustrates the performance variation trends of the SkyLink method after fine-tuning with training data of varying scales (with the x-axis representing the proportion of training samples relative to the total sample size, and the y-axis corresponding to the performance metric R@1). The results demonstrate that the accuracy of SkyLink exhibits a stable and continuous upward trend as the training data scale expands, highlighting its superior scalability and generalization capabilities. To further validate data efficiency, the experiments also plot the performance curve of the retriever Sample4geo. Even with fine-tuning using only 20% of the samples, SkyLink still yields a significant performance increase over the retriever, fully corroborating the high data efficiency advantage of the proposed model, i.e., it requires only limited supervisory signals to effectively enhance the performance of the retriever.

3.6 Case Study

To intuitively verify the effectiveness of SkyLink, a qualitative case analysis is presented in Figure 4. The upper part of this figure displays the Top-5 retrieval results retrieved by the Sample4geo retrieval model. It can be observed intuitively that while the Sample4geo model retrieves results with relatively high semantic similarity, it still faces significant challenges in handling ambiguous samples. Furthermore, starting from the third retrieved image, the discrepancy between its semantic features and those of the query image increases remarkably, which fails to meet the core requirement of sample relevance for geolocalization tasks. The lower part of the figure presents the results after re-ranking by SkyLink. Experimental results demonstrate that the SkyLink model can not only effectively distinguish between highly similar positive samples and semi-positive samples, but also accurately retrieve satellite images with semantic features similar to those of the query image in terms of architectural style, feature combination (of ground objects), and geometric correlation of roads. This result fully confirms that SkyLink possesses robust geospatial semantic understanding capabilities and efficient re-ranking performance.

Furthermore, to rigorously validate the effectiveness of the SkyLink similarity-driven soft labeling strategy, we conducted a specialized case study on ambiguous samples within the University-1652 training set. Please refer to Appendix A.7 for details.

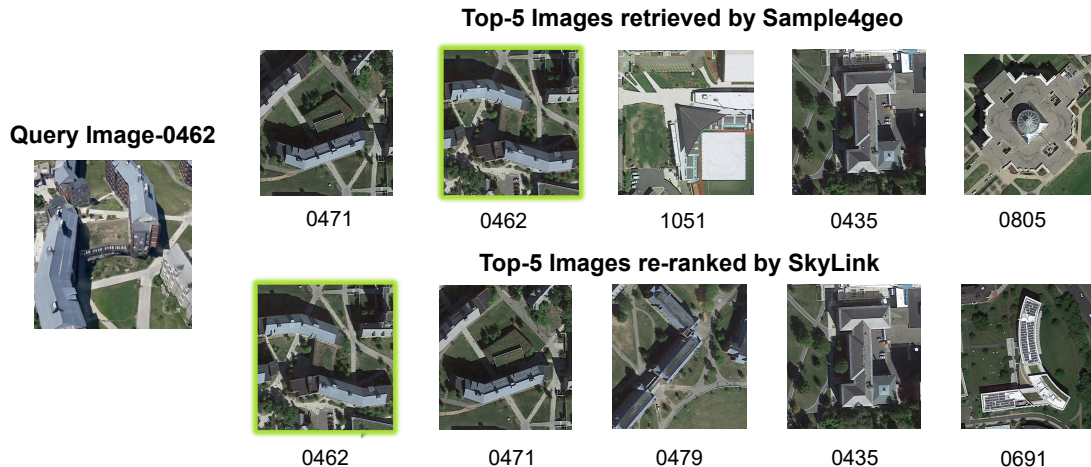


Figure 4: Case Study on the Effectiveness of SkyLink in Candidate Re-Ranking.

4 Related Work

4.1 Cross-View UAV Geolocalization

Cross-view geolocalization is a challenging computer vision task that aims to determine the geographic location of a query image from one perspective (e.g., ground or aerial) by matching it against a database of geo-referenced images from another perspective (typically satellite) [9, 26]. Unmanned Aerial Vehicle (UAV) geolocalization [15] is a particularly demanding subset of this problem [1, 31], characterized by the significant domain gap between oblique-angle UAV imagery and top-down satellite views, which introduces drastic variations in scale, appearance, and geometry. Recent approaches predominantly utilize deep learning to learn viewpoint-invariant feature representations. A prominent research direction focuses on feature partitioning strategies that divide high-level feature maps to capture both fine-grained local details and broader contextual information [31]. MFRGN [32], employ a dual-flow structure to explicitly model multi-scale global and local information, enhancing generalization to new environments. Alongside feature engineering, advancements in network architectures and training paradigms have been crucial. GeoFormer [1], for example, uses an efficient Transformer-based Siamese network with multi-scale feature aggregation. Another key area of innovation is the training process itself. Sample4Geo [13] have pioneered the use of hard negative sampling strategies, using either geographical distance or visual similarity to improve the effectiveness of contrastive learning with the InfoNCE loss. While these methods have significantly advanced feature extraction and training strategies, they still largely depend on separate encoders and naive similarity metrics for the final retrieval, which can fail to capture complex cross-view relationships. In contrast, our proposed method leverages a LVM to jointly model the cross-view interaction between UAV and satellite views, aiming to better capture their complex semantic and spatial relationships for a more accurate final ranking.

4.2 Large Vision-Language Models

Large Vision-Language Models (LVLMs) [33] emerged to address the absence of visual understanding in Large Language Models (LLMs) [34], enabling them to process and comprehend multimodal inputs comprising both images and text. A milestone in this progression was the introduction of CLIP (Contrastive Language-Image Pre-training) [35] by OpenAI. Through contrastive learning on billions of image-text pairs, CLIP aligns visual and textual features within a shared embedding space. This approach facilitates zero-shot image classification by matching images to corresponding text descriptions, laying the groundwork for subsequent multimodal research. Building on this foundation, a new generation of models such as BLIP [36], LLaVA [37], Flamingo [38], and Qwen-VL [30] has further advanced the field. The continuous improvements of these LVLMs in cross-modal reasoning and feature representation make them particularly well-suited for complex tasks like cross-view geolocalization.

4.3 Learning to Rank

Learning-to-Rank (LTR) [39] is a cornerstone technique in information retrieval [40] and recommender systems [41], dedicated to training ranking models that optimize the ordering of candidate items in response to a given query [42]. LTR methodologies are commonly categorized into three paradigms: pointwise [43, 44], pairwise [45, 46], and

listwise [47, 48]. The pointwise approach independently predicts relevance scores for individual query–document pairs; the pairwise paradigm models relative preferences between document pairs; and the listwise framework directly optimizes a global loss function over the entire candidate list. Building upon the LTR framework, this paper explicitly incorporates spatial relationships among samples in the UAV geographic information retrieval dataset by introducing a similarity threshold, thereby achieving effective re-ranking.

5 Conclusion

In this paper, we propose SkyLink, a plug-and-play LVLM-based re-ranking framework that enhances cross-view UAV geolocalization. To better distinguish ambiguous samples, it employs a dynamic relation-aware loss function with cosine similarity soft labeling for semantic capture. We also introduce SkyRank, the dataset for this re-ranking task. Experiments on University-1652 and SUES-200 show SkyLink boosts retriever performance, outperforming baselines in effectiveness and robustness.

References

- [1] Qingge Li, Xiaogang Yang, Jiwei Fan, Ruitao Lu, Bin Tang, Siyu Wang, and Shuang Su. Geoforner: An effective transformer-based siamese network for uav geolocalization. *IEEE Journal of Selected Topics in Applied Earth Observations and Remote Sensing*, 17:9470–9491, 2024. 2, 10
- [2] Robert J. Aughey. Applications of gps technologies to field sports. *International Journal of Sports Physiology and Performance*, 6(3):295–310, 2011. 2
- [3] Jiedong Zhuang, Ming Dai, Xuruoyan Chen, and Enhui Zheng. A faster and more effective cross-view matching method of uav and satellite images for uav geolocalization. *Remote Sensing*, 13(19):3979, 2021. 2
- [4] Nathan Augusto Zacarias Xavier, Elcio Hideiti Shiguemori, and Marcos Ricardo Omena de Albuquerque Maximo. Opencv: A robust framework for aerial navigation under global positioning system denied conditions. *Journal of Aerospace Technology and Management*, 18:e0526, 2026. 2
- [5] Hao Li, Fabian Deuser, Wenping Yin, Steffen Knoblauch, Wufan Zhao, Filip Biljecki, Yong Xue, and Wei Huang. Towards generative location awareness for disaster response: A probabilistic cross-view geolocalization approach. *arXiv preprint arXiv:2512.20056*, 2025. 2
- [6] Hao Li, Fabian Deuser, Wenping Yin, Xuanshu Luo, Paul Walther, Gengchen Mai, Wei Huang, and Martin Werner. Cross-view geolocalization and disaster mapping with street-view and vhr satellite imagery: A case study of hurricane ian. *ISPRS Journal of Photogrammetry and Remote Sensing*, 220:841–854, 2025. 2
- [7] Lei Deng, Zhihui Mao, Xiaojuan Li, Zhuowei Hu, Fuzhou Duan, and Yanan Yan. Uav-based multispectral remote sensing for precision agriculture: A comparison between different cameras. *ISPRS journal of photogrammetry and remote sensing*, 146:124–136, 2018. 2
- [8] Zixuan Song, Jing Zhang, Di Wang, Zidie Zhou, Wenbin Liu, Haonan Guo, En Wang, and Bo Du. Geobridge: A semantic-anchored multi-view foundation model bridging images and text for geo-localization. *arXiv preprint arXiv:2512.02697*, 2025. 2
- [9] Abhilash Durgam, Sidike Paheding, Vikas Dhiman, and Vijay Devabhaktuni. Cross-view geo-localization: a survey. *IEEE Access*, 2024. 2, 4, 10
- [10] Panwang Xia, Yi Wan, Zhi Zheng, Yongjun Zhang, and Jiwei Deng. Enhancing cross-view geo-localization with domain alignment and scene consistency. *IEEE Transactions on Circuits and Systems for Video Technology*, 34(12):13271–13281, 2024. 2
- [11] Qiong Wu, Yi Wan, Zhi Zheng, Yongjun Zhang, Guangshuai Wang, and Zhenyang Zhao. Camp: A cross-view geo-localization method using contrastive attributes mining and position-aware partitioning. *IEEE Transactions on Geoscience and Remote Sensing*, 62:1–14, 2024. 2
- [12] Xiangzeng Liu, Ziyao Wang, Yue Wu, and Qiguang Miao. Segcn: A semantic-aware graph convolutional network for uav geo-localization. *IEEE Journal of Selected Topics in Applied Earth Observations and Remote Sensing*, 17:6055–6066, 2024. 2
- [13] Fabian Deuser, Konrad Habel, and Norbert Oswald. Sample4geo: Hard negative sampling for cross-view geo-localisation. In *Proceedings of the IEEE/CVF International Conference on Computer Vision (ICCV)*, pages 16847–16856, October 2023. 2, 4, 6, 10

- [14] Royston Rodrigues and Masahiro Tani. Semgeo: Semantic keywords for cross-view image geo-localization. In *ICASSP 2023-2023 IEEE International Conference on Acoustics, Speech and Signal Processing (ICASSP)*, pages 1–5. IEEE, 2023. 2, 4
- [15] Yuxiang Ji, Boyong He, Zhuoyue Tan, and Liaoni Wu. Game4loc: A uav geo-localization benchmark from game data. In *Proceedings of the AAAI Conference on Artificial Intelligence*, volume 39, pages 3913–3921, 2025. 2, 10
- [16] Jinglin Huang, Maoqiang Wu, Peichun Li, Wen Wu, and Rong Yu. Vimgeo: Efficient cross-view geo-localization with vision mamba architecture. In *Proceedings of the Thirty-Fourth International Joint Conference on Artificial Intelligence*, pages 1188–1196, 2025. 2
- [17] Peipei Xia, Li Zhang, and Fanzhang Li. Learning similarity with cosine similarity ensemble. *Information Sciences*, 2015. 2
- [18] Aaron van den Oord, Yazhe Li, and Oriol Vinyals. Representation learning with contrastive predictive coding. *arXiv preprint arXiv:1807.03748*, 2018. 2
- [19] Florian Schroff, Dmitry Kalenichenko, and James Philbin. Facenet: A unified embedding for face recognition and clustering. In *Proceedings of the IEEE conference on computer vision and pattern recognition*, pages 815–823, 2015. 2
- [20] Quan Chen, Tingyu Wang, Zihao Yang, Haoran Li, Rongfeng Lu, Yaoqi Sun, Bolun Zheng, and Chenggang Yan. Sdpl: Shifting-dense partition learning for uav-view geo-localization. *IEEE Transactions on Circuits and Systems for Video Technology*, 34(11):11810–11824, 2024. 2, 6
- [21] Tianrui Shen, Yingmei Wei, Lai Kang, Shanshan Wan, and Yee-Hong Yang. Mccg: A convnext-based multiple-classifier method for cross-view geo-localization. *IEEE Transactions on Circuits and Systems for Video Technology*, 34(3):1456–1468, 2023. 2, 6
- [22] Zhedong Zheng, Yunchao Wei, and Yi Yang. University-1652: A multi-view multi-source benchmark for drone-based geo-localization. In Chang Wen Chen, Rita Cucchiara, Xian-Sheng Hua, Guo-Jun Qi, Elisa Ricci, Zhengyou Zhang, and Roger Zimmermann, editors, *MM '20: The 28th ACM International Conference on Multimedia, Virtual Event / Seattle, WA, USA, October 12-16, 2020*, pages 1395–1403. ACM, 2020. 2, 5
- [23] Runzhe Zhu, Ling Yin, Mingze Yang, Fei Wu, Yuncheng Yang, and Wenbo Hu. SUES-200: A multi-height multi-scene cross-view image benchmark across drone and satellite. *IEEE Trans. Circuits Syst. Video Technol.*, 33(9):4825–4839, 2023. 2, 5
- [24] Edward J Hu, Yelong Shen, Phillip Wallis, Zeyuan Allen-Zhu, Yuanzhi Li, Shean Wang, Lu Wang, Weizhu Chen, et al. Lora: Low-rank adaptation of large language models. *ICLR*, 1(2):3, 2022. 4
- [25] Li Mi, Chang Xu, Javiera Castillo-Navarro, Syrielle Montariol, Wen Yang, Antoine Bosselut, and Devis Tuia. Congeo: Robust cross-view geo-localization across ground view variations. In *European Conference on Computer Vision*, pages 214–230. Springer, 2024. 4
- [26] Danilo Avola, Luigi Cinque, Emad Emam, Federico Fontana, Gian Luca Foresti, Marco Raoul Marini, Alessio Mecca, and Daniele Pannone. Uav geo-localization for navigation: A survey. *IEEE Access*, 2024. 4, 10
- [27] Ilya Loshchilov and Frank Hutter. Decoupled weight decay regularization. *arXiv preprint arXiv:1711.05101*, 2017. 6
- [28] Bo Li, Yuanhan Zhang, Dong Guo, Renrui Zhang, Feng Li, Hao Zhang, Kaichen Zhang, Peiyuan Zhang, Yanwei Li, Ziwei Liu, et al. Llava-onevision: Easy visual task transfer. *arXiv preprint arXiv:2408.03326*, 2024. 9
- [29] Jinze Bai, Shuai Bai, Yunfei Chu, Zeyu Cui, Kai Dang, Xiaodong Deng, Yang Fan, Wenbin Ge, Yu Han, Fei Huang, et al. Qwen technical report. *arXiv preprint arXiv:2309.16609*, 2023. 9
- [30] Peng Wang, Shuai Bai, Sinan Tan, Shijie Wang, Zhihao Fan, Jinze Bai, Keqin Chen, Xuejing Liu, Jialin Wang, Wenbin Ge, Yang Fan, Kai Dang, Mengfei Du, Xuancheng Ren, Rui Men, Dayiheng Liu, Chang Zhou, Jingren Zhou, and Junyang Lin. Qwen2-vl: Enhancing vision-language model’s perception of the world at any resolution. *arXiv preprint arXiv:2409.12191*, 2024. 9, 10
- [31] Quan Chen, Tingyu Wang, Rongfeng Lu, Yu Liu, Bolun Zheng, and Zhedong Zheng. Scale-adaptive uav geo-localization via height-aware partition learning. *arXiv preprint arXiv:2412.11535*, 2024. 10
- [32] Yuntao Wang, Jinpu Zhang, Ruonan Wei, Wenbo Gao, and Yuehuan Wang. Mfrgn: Multi-scale feature representation generalization network for ground-to-aerial geo-localization. In *Proceedings of the 32nd ACM International Conference on Multimedia*, pages 2574–2583, 2024. 10
- [33] Jingyi Zhang, Jiaying Huang, Sheng Jin, and Shijian Lu. Vision-language models for vision tasks: A survey. *IEEE transactions on pattern analysis and machine intelligence*, 46(8):5625–5644, 2024. 10

- [34] Wayne Xin Zhao, Kun Zhou, Junyi Li, Tianyi Tang, Xiaolei Wang, Yupeng Hou, Yingqian Min, Beichen Zhang, Junjie Zhang, Zican Dong, et al. A survey of large language models. *arXiv preprint arXiv:2303.18223*, 1(2), 2023. 10
- [35] Alec Radford, Jong Wook Kim, Chris Hallacy, Aditya Ramesh, Gabriel Goh, Sandhini Agarwal, Girish Sastry, Amanda Askell, Pamela Mishkin, Jack Clark, Gretchen Krueger, and Ilya Sutskever. Learning transferable visual models from natural language supervision. In Marina Meila and Tong Zhang, editors, *Proceedings of the 38th International Conference on Machine Learning, ICML 2021, 18-24 July 2021, Virtual Event*, volume 139 of *Proceedings of Machine Learning Research*, pages 8748–8763. PMLR, 2021. 10
- [36] Junnan Li, Dongxu Li, Caiming Xiong, and Steven C. H. Hoi. BLIP: bootstrapping language-image pre-training for unified vision-language understanding and generation. In Kamalika Chaudhuri, Stefanie Jegelka, Le Song, Csaba Szepesvári, Gang Niu, and Sivan Sabato, editors, *International Conference on Machine Learning, ICML 2022, 17-23 July 2022, Baltimore, Maryland, USA*, volume 162 of *Proceedings of Machine Learning Research*, pages 12888–12900. PMLR, 2022. 10
- [37] Haotian Liu, Chunyuan Li, Qingyang Wu, and Yong Jae Lee. Visual instruction tuning. *Advances in neural information processing systems*, 36:34892–34916, 2023. 10
- [38] Jean-Baptiste Alayrac, Jeff Donahue, Pauline Luc, Antoine Miech, Iain Barr, Yana Hasson, Karel Lenc, Arthur Mensch, Katherine Millican, Malcolm Reynolds, et al. Flamingo: a visual language model for few-shot learning. In *Advances in Neural Information Processing Systems (NeurIPS)*, volume 35, pages 23716–23736, 2022. 10
- [39] Zhe Cao, Tao Qin, Tie-Yan Liu, Ming-Feng Tsai, and Hang Li. Learning to rank: From pairwise approach to listwise approach. In *Proceedings of the 24th International Conference on Machine Learning (ICML)*, pages 129–136, Corvallis, Oregon, USA, 2007. ACM. 10
- [40] Tie-Yan Liu. Learning to rank for information retrieval. *Foundations and Trends® in Information Retrieval*, 3(3):225–331, 2009. 10
- [41] Alexandros Karatzoglou, Linas Baltrunas, and Yue Shi. Learning to rank for recommender systems. In *Proceedings of the 7th ACM Conference on Recommender Systems (RecSys)*, pages 493–494, Hong Kong, China, 2013. ACM. 10
- [42] Md Ahsanul Kabir, Mohammad Al Hasan, Aritra Mandal, Daniel Tunkelang, and Zhe Wu. A survey on e-commerce learning to rank, December 2024. arXiv preprint. 10
- [43] Anthony Bell, Prathyusha Senthil Kumar, and Daniel Miranda. The title says it all: a title term weighting strategy for ecommerce ranking. In *Proceedings of the 27th ACM International Conference on Information and Knowledge Management*, pages 2233–2241, 2018. 10
- [44] Siamak Zamani Dadaneh, Shahin Boluki, Mingyuan Zhou, and Xiaoning Qian. Arsm gradient estimator for supervised learning to rank. In *ICASSP 2020-2020 IEEE International Conference on Acoustics, Speech and Signal Processing (ICASSP)*, pages 3157–3161. IEEE, 2020. 10
- [45] Yukihiko Tagami, Shingo Ono, Koji Yamamoto, Koji Tsukamoto, and Akira Tajima. Ctr prediction for contextual advertising: Learning-to-rank approach. In *Proceedings of the Seventh International Workshop on Data Mining for Online Advertising*, pages 1–8, 2013. 10
- [46] Mattia Cerrato, Marius Köppel, Alexander Segner, Roberto Esposito, and Stefan Kramer. Fair pairwise learning to rank. In *2020 IEEE 7th International Conference on Data Science and Advanced Analytics (DSAA)*, pages 729–738. IEEE, 2020. 10
- [47] Christopher J. C. Burges. From RankNet to LambdaRank to LambdaMART: An overview. *Journal of Machine Learning Research: Workshop and Conference Proceedings*, 11:81, 2010. Workshop on Learning to Rank. 11
- [48] Fen Xia, Tie-Yan Liu, Jue Wang, Wensheng Zhang, and Hang Li. Listwise approach to learning to rank: theory and algorithm. In *Proceedings of the 25th international conference on Machine learning*, pages 1192–1199, 2008. 11

A Appendix

A.1 Datasets and Evaluation Metrics

Table 3: Details of datasets for experiment.

DATASETS	SUES-200	UNIVERSITY-1652
PLATFORM	DRONE, SATELLITE	DRONE, GROUND, SATELLITE
TARGET	DIVERSITY	BUILDING
HEIGHT DIFFERENCE	TRUE	FALSE
TRAINING SET	6120	50218
IMAGES/LOCATION	50 + 1	54 + 16.64 + 1

We conduct experiments on two datasets for cross-view geolocation tasks: University-1652 and SUES-200, as shown in Table 3. Performance is evaluated using Recall and Average Precision (AP) as the assessment metrics.

To quantify the optimization efficacy of the proposed re-ranking strategy in a more scientific and precise manner, the evaluation sample set is partitioned into retrieval sets containing positive samples and those devoid of positive samples when computing AP. For retrieval sets with positive samples, the conventional AP calculation is employed. In contrast, for retrieval sets lacking positive samples, a conservative approach is adopted by assigning an AP value of zero. This methodology yields a lower overall AP compared to the full-set computation, thereby providing a more conservative performance estimate and further underscoring the objectivity and rigor of the re-ranking evaluation process.

A.2 SkyRank Dataset

This study constructs the first dataset for training candidate ranking models in cross-view geolocation, with a total of 5 sub-datasets built to cover the data distributions of University-1652 and SUES-200, as illustrated in Table 4.

A.3 The Introduction of Retrievers

SDPL introduces a shifting-dense partition strategy that divides images into dense parts while preserving global structure. A shifting-fusion mechanism generates multiple part sets from varied centers and adaptively fuses features, enhancing robustness to target shifts and scale variations.

Sample4Geo adopts a compact contrastive pipeline with symmetric InfoNCE loss, bypassing aggregation modules and preprocessing. It introduces dual hard-negative mining via geographic proximity and embedding similarity, enhancing feature discrimination.

MCCG builds on ConvNeXt, using cross-dimensional interaction to yield multiple discriminative representations. This design captures extensive contextual details, overcoming information loss in global or segmented features.

Table 4: Query Images and Corresponding Top 10 Gallery Matches.

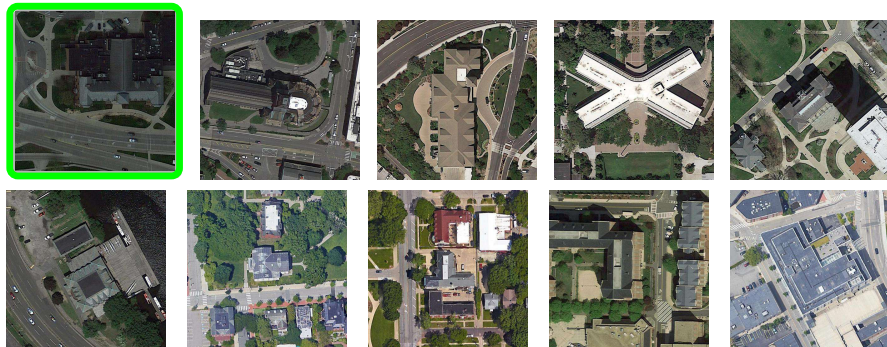
Query Image	Top 10 Gallery Matches
	

Table 5: Parameter setting.

PARAMETER	VALUE
TRAINING TIME (UNIV-1652)	13 HOURS / EPOCH
TRAINING TIME (SUES-200)	4 HOURS / EPOCH
VLM MODEL	QWEN2-VL-7B
DEEPSPEED	STAGE 2
GPU MEMORY CONSUMPTION	30 GB / GPU
BATCH SIZE PER DEVICE	1
LORA RANK	16
SCALING FACTOR	32
LORA DROPOUT	0.05
LEARNING RATE	10^{-4}
BATCH SIZE	4
TRAINING EPOCH	1

Table 6: Sensitivity analysis of hyperparameter T on the SUES-200 dataset.

METHOD	SUES-150		SUES-200		SUES-250		SUES-300	
	R@1 \uparrow	AP \uparrow						
SAMPLE4GEO	92.87	95.58	94.47	96.79	96.83	98.17	97.40	98.16
+SKYLINK ($T = 0.9$)	95.77	97.51	96.45	98.02	97.75	98.70	97.62	98.76
+SKYLINK ($T = 1.0$)	95.20	97.10	95.95	97.84	97.98	98.93	98.92	99.41

A.4 More Details on Training and Inference

Our experiments are divided into two phases: training and inference. The training phase experiments were conducted on 2 NVIDIA A100 GPUs, while the inference phase was performed on 1 NVIDIA A100 GPU. The results indicate that in the University-1652, each training epoch requires approximately 13 hours, while in the SUES-200 single-altitude level, each training epoch takes about 4 hours, with a single-device GPU memory consumption of approximately 60 GB in both cases. (Refer to Table 5)

A.5 More Details on Hyperparameter Analysis

Extensive experiments were conducted on the SUES-200 dataset to validate the model performance. Experimental results demonstrate that when the hyperparameter T approaches 1, the rate of performance improvement of the model slows down in the challenging task of low-altitude UAV image retrieval from satellite imagery. In contrast, for the high-altitude target retrieval task, the heterogeneity of the reference image set shows an upward trend, while the requirement for processing ambiguous samples during the training phase decreases accordingly. Ultimately, this leads to a more significant performance improvement of the model in this specific task scenario. (Refer to Table 6)

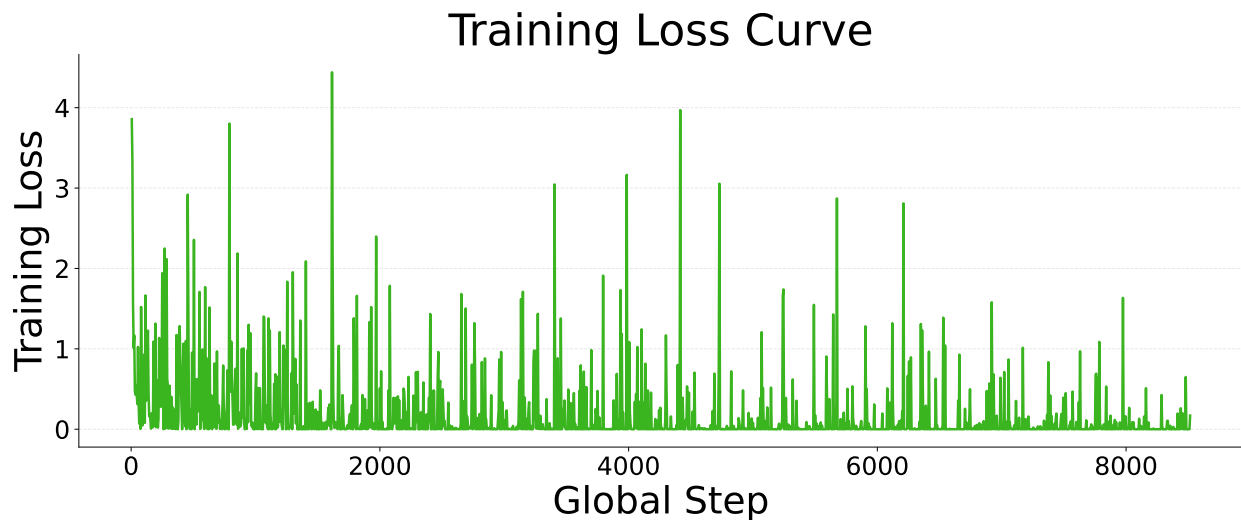
Furthermore, through sensitivity analysis, we identified a set of optimal hyperparameter configurations that can maximize the re-ranking potential of the large model ($|G_z| = 13$, $|\text{top-k}| = 10$, $T = 0.9$).

A.6 The Supplement of Ablation Study

After removing the similarity threshold mechanism from the model (i.e., w/o similarity threshold), we observed severe fluctuations in the loss value throughout the model training process via the experimental training monitoring platform W&B. (Figure 5) This result reveals that simply using the first reference sample directly as the label for training (i.e., without screening and optimizing labels through the similarity threshold) will have a devastating impact on the model’s ability to process similar samples.



(a) Training loss of the model (with similarity threshold)



(b) Training loss of the model (without similarity threshold)

Figure 5: Comparison of training loss with and without similarity threshold

A.7 Case Study on Soft Labels

To rigorously evaluate the efficacy of SkyLink’s similarity-based soft labeling mechanism, we conducted a targeted case study on ambiguous samples from the University-1652 training set, as illustrated in Figure 6. For a given query image, the original hard label designates only the top-ranked reference image as the positive sample, thereby overlooking the supervisory potential of visually similar yet ambiguous instances. These ambiguous samples typically correspond to different orientations or viewpoints of the same geographic region. By employing soft labeling, additional discriminative signals can be effectively harnessed from such instances. Specifically, with the similarity threshold set at 0.9, samples exceeding this threshold are assigned positive soft labels proportional to their cosine similarity scores, whereas those below the threshold receive zero labels. This mechanism enables SkyLink to reliably propagate pseudo-labels to visually akin but label-ambiguous drone-view and satellite-view instances, thereby substantially mitigating label noise and enhancing cross-view geo-localization performance.

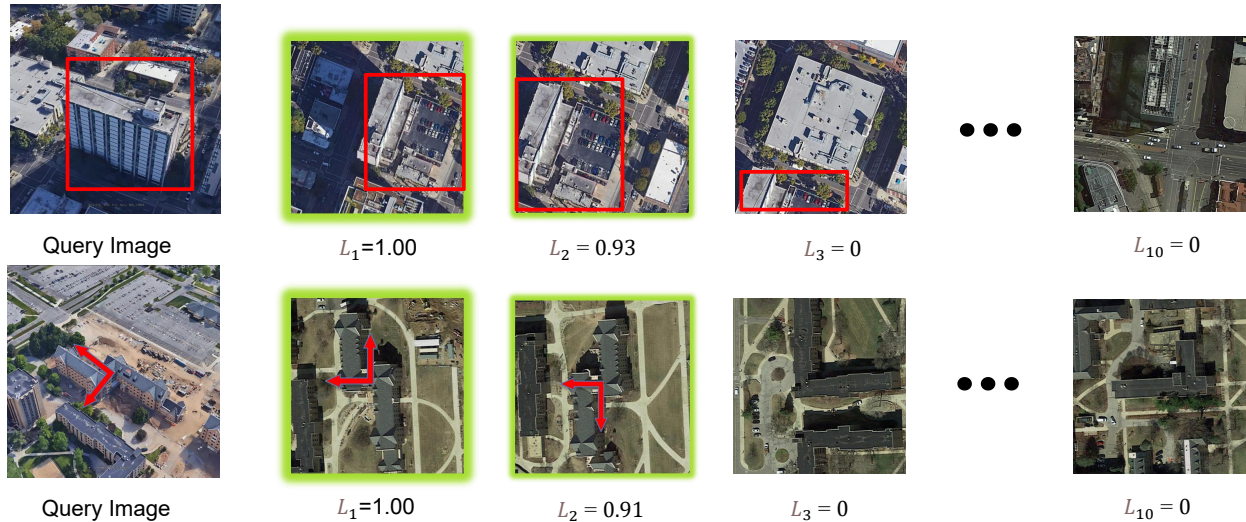


Figure 6: Case Study on the similarity labels of SkyLink.

A.8 The prompt of prompt-based method

In our baseline, the large vision-language model (VLM) is prompted with a multi-image context that includes one query image and up to top-k candidate reference images. The model is instructed to assign a relevance score between 0 and 10 for each candidate relative to the query. The core prompt template can be abstracted as:

```

{query image}
This is the query image above. Now, here are {k} candidate reference images. For each candidate, evaluate how well it matches the query image on a scale from 0 (no match) to 10 (perfect match).
{candidate image 1}
{candidate image 2}
⋮
{candidate image k}
Output only the scores in this exact format:
Candidate 1: {score}
Candidate 2: {score}
⋮
Candidate k: {score}
Do not add any other text or explanation.
    
```

A.9 Algorithm

SkyLink is a retrieval-augmented generative framework that aligns visual-semantic representations through contrastive supervision derived from a vision-language model (VLM). During training, for each query image I_q , SkyLink constructs a context set \mathcal{K} comprising the ground-truth target I_{gt} and $k - 1$ top candidates from a coarse retrieval pool \mathcal{C}'_q . A lightweight LoRA-adapted large vision-language model ($\mathcal{M}_{\text{LoRA}}$) processes multimodal prompts formed by pairing I_q with each candidate in \mathcal{K} , producing last-layer embeddings that are scored via a learnable linear head w . These scores are supervised by soft labels L_j computed as thresholded cosine similarities between retrieved and ground-truth image embeddings from a frozen dual-encoder retriever (E_q, E_r), enabling gradient-based optimization of both LoRA parameters and the scoring head. At inference, SkyLink first retrieves the top- m candidates from a large reference corpus \mathcal{R} using E_q , then re-ranks them by prompting $\mathcal{M}_{\text{SkyLink}}$ with each candidate and selecting the one yielding the highest score.

Algorithm 1 SkyLink: Training and Inference**Require:**

- Training: $\mathcal{D}_{\text{train}} = \{(I_q, C'_q, I_{gt})\}$, retriever (E_q, E_r) , LVLM \mathcal{M} , LoRA rank r , k , threshold T
- Inference: $I_q, \mathcal{R} = \{I_r^i\}_{i=1}^N, V_R = \{E_r(I_r^i)\}, \mathcal{M}_{\text{SkyLink}}, m$

Ensure: \hat{I} **Training Stage**

- 1: **procedure** TRAINSKYLINK($\mathcal{D}_{\text{train}}, \mathcal{M}, E_r, k, T, r$)
- 2: Initialize LoRA $\{A_l, B_l\}_{l=1}^L$ in \mathcal{M}
- 3: **for each** $(I_q, C'_q, I_{gt}) \in \mathcal{D}_{\text{train}}$ **do**
- 4: $\mathcal{K} \leftarrow \{I_{gt}\} \cup \text{top-}(k-1)(C'_q)$ ▷ $|\mathcal{K}| = k$
- 5: $\mathcal{P} \leftarrow \{\text{Prompt}(I_q, I_c) \mid I_c \in \mathcal{K}\}$
- 6: $h[\text{last}] \leftarrow \mathcal{M}_{\text{LoRA}}(\mathcal{P})[-1] \in \mathbb{R}^{k \times d}$
- 7: $S \leftarrow w^\top h[\text{last}] \in \mathbb{R}^k$
- 8: $L_j \leftarrow \max\left(0, \frac{E_r(I_{c_j})^\top E_r(I_{gt})}{\|E_r(I_{c_j})\| \|E_r(I_{gt})\|} - T\right)$ for $j = 1$ to k ▷ Soft labels via cosine sim
- 9: $\mathcal{L} \leftarrow -\frac{1}{k} \sum_{j=1}^k [L_j \log \sigma(S_j) + (1 - L_j) \log(1 - \sigma(S_j))]$
- 10: Update LoRA $\{A_l, B_l\}$ and w via $\nabla \mathcal{L}$
- 11: **end for**
- 12: **return** $\mathcal{M}_{\text{SkyLink}}$
- 13: **end procedure**

Inference Stage

- 14: **procedure** INFERSKYLINK($I_q, \mathcal{R}, V_R, \mathcal{M}_{\text{SkyLink}}, m$)
- 15: $v_q \leftarrow E_q(I_q)$
- 16: $C_q \leftarrow \text{top-}m(V_R, v_q)$ ▷ Retrieve via cosine similarity
- 17: $s \leftarrow \mathcal{M}_{\text{SkyLink}}(\text{Prompt}(I_q, I_c))$ for each $I_c \in C_q$
- 18: **return** $\hat{I} \leftarrow \arg \max_{I_c \in C_q} s[I_c]$
- 19: **end procedure**

A.10 Limitation

SkyLink achieves significant improvements in the accuracy and robustness of cross-view UAV geolocalization, particularly through its dynamic relation-aware loss function and the SkyRank dataset. However, the method is not without limitations. The plug-and-play framework adopted by SkyLink introduces an additional re-ranking stage, which significantly increases computational overhead during inference compared to direct embedding-based retrieval methods. Currently, this added complexity constrains its deployment on airborne platforms, often necessitating reliance on ground stations for processing. This poses substantial practical challenges in resource-constrained environments or applications with stringent real-time requirements. Future work could explore the development of end-to-end ranking approaches to mitigate this issue. Furthermore, as a re-ranking mechanism, SkyLink’s performance is strictly bounded by the recall of the initial retrieval stage. The model can only re-rank candidates provided by the base retriever. If the ground truth is not present within the top- N candidates (where $N = 10$ in our inference setting), SkyLink cannot recover the correct match. Consequently, the theoretical upper bound of our method is determined by the Retriever’s $R@N$. As shown in our experiments, the theoretical ceiling is capped at 98.13% (the $R@10$ of the base retriever). Future efforts should focus on developing more advanced retrievers to improve this initial recall ceiling or expanding the candidate pool size N , albeit at the cost of increased computational load.